



Alexandria University
Alexandria Engineering Journal

www.elsevier.com/locate/aej
www.sciencedirect.com



ORIGINAL ARTICLE

Numerical passive control of alumina nanoparticles in purely aquatic medium featuring EMHD driven non-Darcian nanofluid flow over convective Riga surface



Ghulam Rasool^{a,b,*}, Abderrahim Wakif^c, Xinhua Wang^{a,*}, Anum Shafiq^d,
 Ali J. Chamkha^e

^a *Institute of Intelligent Machinery, Faculty of Materials and Manufacturing, Beijing University of Technology, Beijing 100124, China*

^b *Department of Mechanical Engineering, Lebanese American University, Beirut Lebanon*

^c *Laboratory of Mechanics, Faculty of Sciences Ain Chock, Hassan II University of Casablanca, Morocco*

^d *School of Mathematics and Statistics, Nanjing University of Information Science and Technology, Nanjing, China*

^e *Faculty of Engineering, Kuwait College of Science and Technology, Doha District 35004, Kuwait*

Received 25 July 2022; revised 23 November 2022; accepted 15 December 2022

Available online 22 December 2022

KEYWORDS

Riga pattern;
 EMHD convective nanofluid flow;
 Alumina water-based nanofluid;
 Darcy-Forchheimer porous medium;
 Buongiorno's model;
 Koo-Kleinstreuer-Li's correlations

Abstract Motivated by the thermal importance of feeble electrically conducting nanofluids and their flow controls in many industrial and engineering applications, the present scrutinization intended to evidence comprehensively the main electro-magneto-hydrothermal and mass aspects of convective non-homogeneous flows of alumina-based pure water nanofluids $Al_2O_3 - H_2O$ over a horizontal flat surface of an electromagnetic actuator (i.e., Riga pattern, which is embedded geometrically in a Darcy-Forchheimer porous medium. Further, the present nanofluid flow model is formulated realistically under the umbrella of the renovated two-phase Buongiorno's approach with the inclusion of Brownian motion and thermophoresis diffusive phenomena, in which the vertical component of the nanoparticles' mass flux tend to vanish at the limiting contact surface due to its impermeability trend. For streamlining the technical handling of the present nanofluid flow problem, the governing partial differential equations (PDEs) are simplified mathematically by adopting the physical approximations of the boundary layer theory and then transformed into a differential structure of ordinary differential equations (ODEs) based on several similarity changes. Methodologically, the resulting nonlinear coupled ODEs are solved numerically via a validated differential quadrature procedure. Besides, the generated graphical demonstrations show that the nanofluid temperature is enhanced significantly with the porosity factors, the nanoparticles' loading, the convective heating strength, and the thermophoresis process. However, the porosity factors and the nanoparticles' loading exhibit a slowing-down impact on the nanofluid motion. Usefully, it

* Corresponding authors.

E-mail addresses: grasool@bjut.edu.cn (G. Rasool), sunxhking@aliyun.com (X. Wang).

Peer review under responsibility of Faculty of Engineering, Alexandria University.

<https://doi.org/10.1016/j.aej.2022.12.032>

1110-0168 © 2022 THE AUTHORS. Published by Elsevier BV on behalf of Faculty of Engineering, Alexandria University.

This is an open access article under the CC BY-NC-ND license (<http://creativecommons.org/licenses/by-nc-nd/4.0/>).

Nomenclature

General Symbols

a_0	Geometrical size of magnets and electrodes, [m]
$\hat{C}_D = C_0 x^{-1}$	Modified drag coefficient, [-]
C_0	Frictional quadrature coefficient, [m]
C_P	Specific heat, [$J kg^{-1} K^{-1}$]
C	Nanoparticles' molar concentration, [$mol m^{-3}$]
C_∞	Nanoparticles' molar concentration at the free-stream region, [$mol m^{-3}$]
d_{np}	Nanoparticles' diameter, ($d_{np} = 47 \times 10^{-9} m$)
(D_B, D_T)	Brownian and thermophoresis diffusive coefficients, [$m^2 s^{-1}$]
$F = \frac{\hat{C}_D}{\sqrt{k}}$	Inertial drag coefficient, [m^{-1}]
h	Convective heat transfer coefficient, [$W m^{-2} K^{-1}$]
$H(\eta)$	Temperature function, [-]
j	Electrical current density, [$A m^{-2}$]
k	Thermal conductivity, [$W m^{-1} K^{-1}$]
$\hat{k}_{np} = \frac{d_{np} k_{np}}{k_{np} R_f + d_{np}}$	Modified thermal conductivity of nanoparticles, [$W m^{-1} K^{-1}$]
k_{np}	Thermal conductivity of nanoparticles, [$W m^{-1} K^{-1}$]
k_B	Boltzmann constant, ($k_B = 1.38066 \times 10^{-23} JK^{-1}$)
K	Permeability of the medium, [m^2]
$M(\eta)$	Concentration function, [-]
$\hat{M} = M_0 x$	Variable magnetization strength, [$kg s^{-2} A^{-1}$]
R_f	Interfacial thermal resistance between the nanoparticles, ($R_f = 4 \times 10^{-8} Km^2 W^{-1}$)
s	Stretching velocity coefficient, [s^{-1}]
$\{S(\eta), S'(\eta)\}$	Velocity functions, [-]
T	Temperature, [K]
T_f	Working fluid Temperature, [K]
T_∞	Temperature at the free-stream region, [K]
$\Delta T = T_f - T_\infty$	Temperature difference, [K]
T_0	Reference temperature, ($T_0 = 300K$)
V	Volume, [m^3]
(u, v)	Velocity components, [$m s^{-1}$]
$U_w = sx$	Linear stretching velocity, [$m s^{-1}$]
(x, y)	Cartesian coordinates, [m]

Greek Symbols

δ_C	Corrective factor, [$mol m^{-3}$]
ϕ	Nanoparticles' volume fraction, [-]
η	Similarity variable, [-]
μ	Dynamic viscosity, [$kg m^{-1} s^{-1}$]
ν	Kinematic viscosity, [$m^2 s^{-1}$]
$H(\eta)$	Temperature function, [-]
ρ	Density, [$kg m^{-3}$]
σ	Electrical conductivity, [$S m^{-1}$]
(ρC_P)	Heat capacitance, [$J m^{-3} K^{-1}$]

Subscripts

bf	Base fluid
nf	Nanofluid
np	Nanoparticles
f	Working fluid
∞	Free-stream condition
w	Surface condition

Superscripts

,	First derivative w.r.t. η
,,	Second derivative w.r.t. η
,,,	Third derivative w.r.t. η

Abbreviations

BCs_C	Mass boundary conditions
BCs_T	Thermal boundary conditions
$BCs_{(u,v)}$	Kinematic boundary conditions
$EMHD$	Electro-magneto-hydrodynamic
$GDQM$	Generalized Differential Quadrature Method
MHD	Magneto-hydrodynamic
NRT	Newton-Raphson Technique
$ODEs$	Ordinary differential equations
$PDEs$	Partial differential equations
$RKFM$	Runge-Kutta-Fehlberg Method
ST	Shooting Technique

is revealed from the obtained GDQM - NRT datasets that the nanoparticles' loading and the porosity factors express an important improvement in the strength of the surface viscous drag forces, whereas the induced electromagnetic field shows a reverse viscous frictional impact.

© 2022 THE AUTHORS. Published by Elsevier BV on behalf of Faculty of Engineering, Alexandria University. This is an open access article under the CC BY-NC-ND license (<http://creativecommons.org/licenses/by-nc-nd/4.0/>).

1. Introduction

Nowadays, the concept of monotype, hybrid, and ternary nanofluids (i.e., one, two, or three kinds of nanosized particles suspended in an appropriate viscous base liquid) becomes very popular among scientific researchers and investigators in the nanotechnological field and nanosciences because of the widespread applications of these kinds of stable biphasic mixtures

in heat and mass transfer processes, nano-chemistry, solar energy, cooling of nuclear systems, heat transfer enhancement, and multiphase flows [1–8]. In this respect, Buongiorno et al. [9] conducted benchmarking experimental analyses to demonstrate the effective contribution of solid nanoparticles toward the thermal improvement of some traditional working viscous fluids, which can be considered as basic hosting liquids (e.g., kerosene, water, molten salt, engine oil, and ethylene glycol) for divers spherical/non-spherical nanomaterials having

enormous thermal performances (e.g., metal/metal oxide nanoparticles, nanodiamond particles nano-graphene, and single-/multi-walled carbon nanotubes) as compared with the liquid phase. Further experimental elucidations concerning the significant role of non-spherical nanoparticles on the augmentation of convective heat transfer coefficients of viscous fluids were done comprehensively by Li et al. [10]. Keeping in mind the strong thermal and optical properties of the binary combination TiN@SiCw, Wen et al. [11] proposed the nanofluidic biphasic mixture TiN@SiCw - C₂H₆O₂ as an enhanced working liquid to improve the photo-thermal performance of solar collectors. In another engineering use of nanofluids, Javidan and Moghadam [12] carried out an experimental examination of the silicon carbide-based pure deionized water as an efficient biphasic mixture cooling of photovoltaic modules across a specified arrangement of orifice nozzle modes

In the past few years, several theoretical assessments and experimental observations [13,14] prove that Fourier's paradox [15] of heat conduction stated at the beginning of the nineteenth century is still questionable as a physical model because of its contradictory results to explain the characteristics of heat transfer exclusively. As an improvement of this classical heat transfer law, Cattaneo's theory [16] suggested the addition of a temporal relaxation impact into the heat flux model, which was developed mathematically thereafter by Christov [17]. Other physical insights on the Cattaneo-Christov theory were discussed exhaustively by Bilal et al. [18] for Williamson fluid flows as well as by Shahzad et al. [19] for non-homogeneous micropolar nanofluid flows. Shah et al. [20] exploited non-Fourier's heat transfer and entropy generation mechanisms to explore the behavior of unsteady MHD thin film flows of second-grade nanofluids conveying carbon nanotubes over a stretching sheet. Ragupathi et al. [21] combined the fundamental Fourier's and Buongiorno's approaches [22] to simulate numerically MHD bioconvective nanofluid flows over an impermeable isothermal bent stretching surface with slip velocity condition. The noticeable influences of metallic and non-metallic nanosized particles on the occurrence of thermal instabilities within various viscous fluidic media were discussed inclusively by Sharma and Wakif [23]. Ramzan et al. [24] linked the Cattaneo-Christov approach with the bioconvection phenomenon to examine Hall current and ion slip influences on non-homogeneous magnetized reactive flows of tangent hyperbolic nanofluids near a stretching sheet. Farooq et al. [25] invoked the aforesaid improved heat transfer theory to scrutinize radiating Carreau nanofluid flows conveying tiny particles and motile microorganisms nearby a vertical stretching sheet in the presence of an exponentially declining heat generation. The temporal retarding feature of the generalized Fourier's and Fick's laws was taken into account by Hafeez et al. [26] to reveal the characteristics of magnetically dissipative flows of upper convected Oldroyd-B nanofluids over a turning disk. Hamad et al. [27] incorporated realistic physical impacts (e.g., thermal radiation, magnetic field, energy activation, bioconversion, and stratification constraints) to scrutinize mixed convective Walters-B nanofluid flows near a vertical stretching flat surface. Recent advanced investigations on non-Newtonian nanofluid flows can be seen in [28–33] and the references therein.

Dynamically, the transition from a laminar flow state to a turbulent regime motion can be adjusted magnetohydrodynamically by applying an extrarenal magnetic field of signifi-

cant strength, which can help in the slowing up of electrically conducting fluid/nanofluid flows in most MHD flow problems. In the frameworks of the imperative findings of Gailitis [34], weak electrically conducting laminar flows can be controlled electro-magneto-hydrodynamically via sophisticated actuators (i.e., Riga patterns) comprising a succession of electrodes and magnets and having the capability of generating strength electromagnetic forces (i.e., Lorentz forces). Practically, Riga plates can be used as advanced electromagnetic materials to minimize the impact of viscous drag forces as well as to rescind the flow separation occurrence. In 1961, Grinberg [35] performed a theoretical study on Riga devices to explore the physical feature of the induced Lorentz forces. As important outcomes, it was demonstrated analytically based on strong theoretical knowledge that the magnitude of the induced Lorentz forces presents an exponential decaying demeanor along the transverse direction according to Grinberg's law, in which a higher electromagnetic strength is exerted near the electromagnetic plate. Besides, the mechanical behaviors of Lorentz forces (i.e., aiding trend or resisting role) can be adjusted technically for flat Riga surfaces based on the sense of the electrical current induced by the electrodes as reported by Wakif et al. [36]. The significance of generalized Fourier's and Fick's laws on the features of convective EMHD nanofluid flows in a Darcy-Forchheimer porous medium was discussed briefly by Rasool et al. [37] along with the resisting tendency of Lorentz forces in the case where the vertical component of the nanoparticles' flux is assumed zero at the Riga pattern. In another geometrical configuration, Abdal et al. [38] evidenced the importance of the existence of an internal heat generation on the heat and mass transfer enhancement during the unsteady reactive motion of tangent hyperbolic nanofluid flows over a non-isothermal Riga wedge. Recently, Naveed et al. [39] assumed the validity of Grinberg's expression for curved Riga surfaces to inspect thermodynamically oscillating MHD dissipative fluid flows in the presence of thermal radiation. In the same context, Abbas et al. [40] adopted the homogeneous nanofluid model with multiple slip conditions for the velocity and temperature to perform a numerical study on the flow of the micropolar hybrid nanofluid (SWCNT + MWCNT) - H₂O over an exponentially stretching curved surface. The effective contribution of ohmic heating and heat generation on the thermal enhancement of slippery EMHD non-homogeneous nanofluid flows over a non-linear stretching Riga plate of an uneven thickness was explicated semi-analytically by Hussain et al. [41] using a consistent homotopic algorithm.

Inspired by the above-cited literature, the present numerical investigation aimed to evidence the main hydrothermal aspects featuring EMHD convective flows of alumina-based pure water nanofluids Al₂O₃ - H₂O, which have not been provided so far as per the author's knowledge. By invoking the advanced Buongiorno's theory under the assumption of the passive control approach (i.e., zero mass flux at the boundary), the motion of the non-homogeneous nanofluidic mixture Al₂O₃ - H₂O is assumed to be driven in a laminar regime over an impermeable horizontal Riga pattern, which is heated convectively and subjected to a linear stretching movement in a Darcy-Forchheimer porous medium. Besides, the significant contributions of thermophoresis and Brownian mechanisms of nanoparticles in the occurred transport phenomena are taken effectively into account during the formulation of the

conservation equations governing the present nanofluid flow model, which are reinforced more realistically with the help of authenticated thermophysical expressions. By applying a robust differential quadrature algorithm, the resulting differential formulation is handled properly to generate precise numerical outcomes. After successful multiple validations, the accurate outputted datasets are presented in the form of tables and figures to facilitate the understanding of the obtained findings by providing compressive answers to the following pending research questions:

- Which physical model can be adapted realistically to simulate EMHD convective boundary layer flows of alumina-based pure water nanofluids $Al_2O_3 - H_2O$ in a nonlinear porous structure using the notion of nanoparticles' molar concentration?
- What is the source of the electrical and magnetic field exerted simultaneously on the developed flow?
- How can express the induced Lorentz forces in the momentum equation when these electromagnetic actions exhibit an aiding dynamical influence?
- How can evaluate reliably the physical features of the studied biphasic mixture $Al_2O_3 - H_2O$?
- Which mathematical transformations can be used to get similar boundary layer solutions?
- Which methodological procedure can provide accurate results?
- How can control the wall concentration during the convective heating process?
- What is the difference between the original Buongiorno's approach and the present nanofluid flow model?
- What are the influences of the involved physical parameters on the flow pattern as well as on the temperature and nanoparticles' concentration throughout the nanofluidic medium?
- How can improve the thermal performance of the nanofluidic medium?
- How can minimize the strength of the surface drag forces?
- What are the hydrothermal appearances of the proposed nanofluid flow problem?

1.1. Physical and mathematical backgrounds

A laminar steady nanofluid flow is developed electro-magneto-hydrodynamically over a convectively heated Riga pattern embedded horizontally in a nonlinear porous medium defined spatially in a Cartesian frame of coordinate system (x, y, z) . Chemically, the nanofluid is assumed to be dilute of non-homogeneous structure (i.e., biphasic mixture) and comprising alumina nanoparticles and pure water as principal ingredients. Dynamically, three boundary layer regions have happened due to the linear stretching motion of the impermeable surface of the Riga pattern as well as the variable temperature and concentration distributions throughout the nanofluidic medium, in which the stretching velocity is given by $U_w = sx$, where s is a positive dimensional physical constant. As physical constraints, the temperature of the heating fluidic medium and its characteristic convective heat transfer coefficient are characterized respectively by T_f and h , whereas the wall nanoparticles' molar concentration C_w is unknown and can be controlled

passively through the existing relation between the wall concentration and temperature gradients. Furthermore, the nanofluidic medium in the free stream region is assumed to be motionless at uniform distributions for the temperature T_∞ and the nanoparticles' molar concentration C_∞ as portrayed schematically in Fig. 1. It is more interesting to mention here that there is a linear relationship between the nanoparticles' molar concentration C and the nanoparticles' volume fraction ϕ in the form $C = \delta_C \phi$, where δ_C is a corrective factor having the dimension of molar concentration.

Under the umbrella of adjusted Buongiorno's nanofluid model [27,37,42–49] and the boundary layer approximations [50], the partial differential equations (PDEs) governing the present EMHD nanofluid flow problem are stated as follows:

$$\frac{\partial u}{\partial x} + \frac{\partial v}{\partial y} = 0, \quad (1)$$

$$u \frac{\partial u}{\partial x} + v \frac{\partial u}{\partial y} = \frac{\mu_{nf}}{\rho_{nf}} \frac{\partial^2 u}{\partial y^2} + \frac{\pi j \hat{M}}{8 \rho_{nf}} e \left(\frac{-xy}{a_0} \right) - \frac{\mu_{nf}}{\rho_{nf} K} u - Fu^2, \quad (2)$$

$$u \frac{\partial T}{\partial x} + v \frac{\partial T}{\partial y} = \frac{k_{nf}}{(\rho C_p)_{nf}} \frac{\partial^2 T}{\partial y^2} + \frac{(\rho C_p)_{np}}{(\rho C_p)_{nf}} \left(\frac{D_B}{\delta_C} \frac{\partial C}{\partial y} + \frac{D_T}{T_\infty} \frac{\partial T}{\partial y} \right) \frac{\partial T}{\partial y}, \quad (3)$$

$$\frac{u}{\delta_C} \frac{\partial C}{\partial x} + \frac{v}{\delta_C} \frac{\partial C}{\partial y} = \frac{D_B}{\delta_C} \frac{\partial^2 C}{\partial y^2} + \frac{D_T}{T_\infty} \frac{\partial^2 T}{\partial y^2}, \quad (4)$$

These above-mentioned PDEs are constrained by the following boundary conditions (BCs):

$$BC_{S(u,v)} : \{u(x, y=0) = U_w = sx, v(x, y=0) = 0, u(x, y \rightarrow \infty) \rightarrow 0\}, \quad (5)$$

$$BC_{S_T} : \left\{ \frac{\partial T}{\partial y}(x, y=0) = \frac{h}{k_{nf}} [T(x, y=0) - T_f], T(x, y \rightarrow \infty) \rightarrow T_\infty \right\}, \quad (6)$$

$$BC_{S_C} : \left\{ \frac{D_B}{\delta_C} \frac{\partial C}{\partial y}(x, y=0) + \frac{D_T}{T_\infty} \frac{\partial T}{\partial y}(x, y=0) = 0, C(x, y \rightarrow \infty) \rightarrow C_\infty \right\}. \quad (7)$$

Based on the partial characteristics of each phase enlisted in Table 1, the effective thermophysical properties of alumina-water-based nanofluids $Al_2O_3 - H_2O$ figured in Eq. (2) and Eq. (3) can be assessed by employing the following mixture laws [51] and Koo-Kleinstreuer-Li's correlations [52,53]: Table 2

$$\rho_{nf} = (1 - \phi) \rho_{bf} + \phi \rho_{np}, \quad (8)$$

$$(\rho C_p)_{nf} = (1 - \phi) (\rho C_p)_{bf} + \phi (\rho C_p)_{np}, \quad (9)$$

$$\left\{ \begin{array}{l} \frac{\mu_{nf}}{\mu_{bf}} = \frac{1}{(1-\phi)^{2.5}} + 5 \times 10^4 \frac{\phi \mu_{bf}}{\mu_{np}} \sqrt{\frac{k_B T_0}{\rho_{np} d_{np}}} [f_{KKL} \ln(T_0) + g_{KKL}], \\ \frac{k_{nf}}{k_{bf}} = 1 + \frac{3\phi (k_{np} - k_{bf})}{(k_{np}^* + 2k_{bf}) - \phi(k_{np}^* - k_{bf})} + 5 \times 10^4 \frac{\phi (\rho C_p)_{bf}}{k_{bf}} \sqrt{\frac{k_B T_0}{\rho_{np} d_{np}}} [f_{KKL} \ln(T_0) + g_{KKL}], \\ f_{KKL} = \gamma_1 + [\gamma_2 \ln(d_{np}) + \gamma_3 \ln(\phi)] + [\gamma_4 \ln(\phi) + \gamma_5 \ln(d_{np})] \ln(d_{np}), \\ g_{KKL} = \gamma_6 + [\gamma_7 \ln(d_{np}) + \gamma_8 \ln(\phi)] + [\gamma_9 \ln(\phi) + \gamma_{10} \ln(d_{np})] \ln(d_{np}) \end{array} \right\}. \quad (10)$$

Through Eqs. (8)–(10), we define the following relative amounts:

$$\left\{ J_1 = \frac{\mu_{nf}}{\mu_{bf}}, J_2 = \frac{\rho_{nf}}{\rho_{bf}}, J_3 = \frac{(\rho C_p)_{nf}}{(\rho C_p)_{bf}}, J_4 = \frac{k_{nf}}{k_{bf}} \right\}. \quad (11)$$

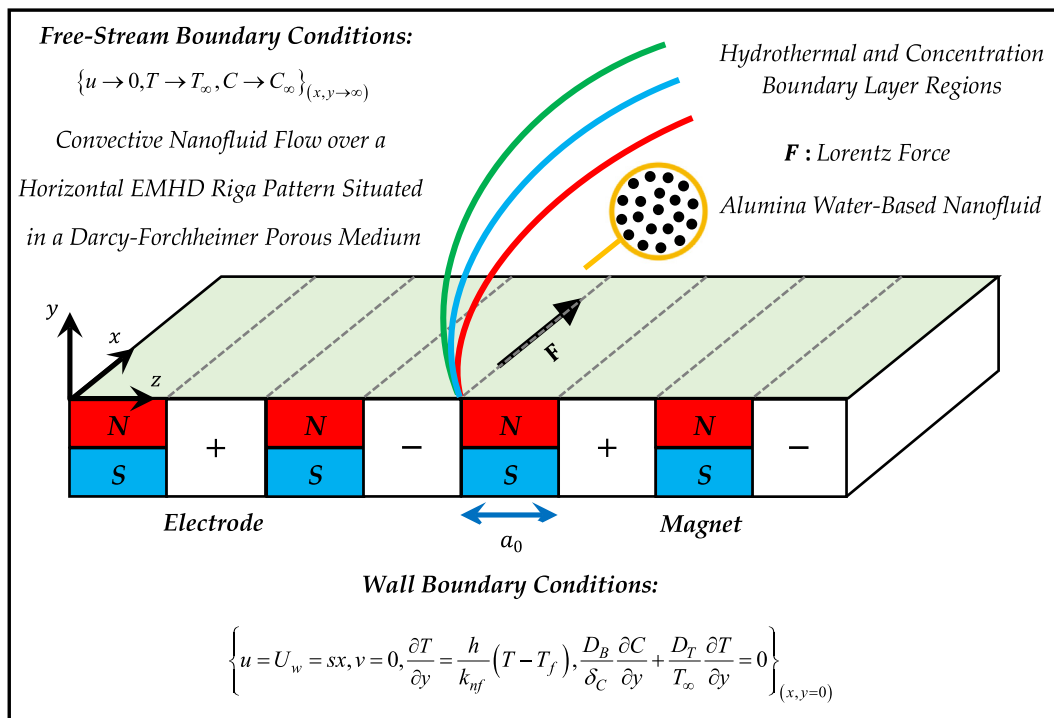


Fig. 1 Geometrical configuration of the nanofluid flow problem.

Table 1 Thermophysical properties of alumina nanoparticles and pure water [53–57].

Properties	ρ ($kg\ m^{-3}$)	C_p ($J\ kg^{-1}\ K^{-1}$)	k ($W\ m^{-1}\ K^{-1}$)	σ ($S\ m^{-1}$)	μ ($\times 10^{-5}\ kg\ m^{-1}\ s^{-1}$)
Alumina	3970	765	40	10^{-10}	—
Water	997.1	4179	0.613	0.05	89

Table 2 Koo-Kleinstreuer-Li’s coefficients for alumina water-based nanofluids [52,53,58].

KKL Coefficients	Values
γ_1	52.813488759
γ_2	6.115637295
γ_3	0.6955745084
γ_4	0.041745552786
γ_5	0.176919300241
γ_6	-298.19819084
γ_7	-34.532716906
γ_8	-3.9225289283
γ_9	-0.2354329626
γ_{10}	-0.999063481

Mathematically, the leading PDEs can be altered to a set of ordinary differential equations (ODEs) by invoking the transformations demonstrated in Table 3.

$$(S) : \left. \begin{aligned} &S(\eta) = 0, S'(\eta) = 1, \text{ when } \eta = 0, \\ &Sm'(\eta) - \lambda S(\eta) + \frac{J_2}{J_1} \left[\begin{matrix} S(\eta) & S'(\eta) \\ (1 + Fr)S'(\eta) & S''(\eta) \end{matrix} \right] + \frac{Ha}{J_1} e^{(-k\eta)} = 0, \text{ when } \eta > 0, \\ &S'(\eta) \rightarrow 0, \text{ as } \eta \rightarrow \infty, \\ &H'(\eta) = \frac{Bi}{J_4} [H(\eta) - 1], \text{ when } \eta = 0, \\ &Hu(\eta) + \frac{Pr}{J_4} [J_3 S(\eta) + NbM'(\eta) + NtH'(\eta)]H'(\eta) = 0, \text{ when } \eta > 0, \\ &H(\eta) \rightarrow 0, \text{ as } \eta \rightarrow \infty, \\ &M'(\eta) + \frac{Nt}{Nb} H'(\eta) = 0, \text{ when } \eta = 0, \\ &Mu(\eta) + \frac{Nt}{Nb} H''(\eta) + ScS(\eta)M'(\eta) = 0, \text{ when } \eta > 0, \\ &M(\eta) \rightarrow 1, \text{ as } \eta \rightarrow \infty \end{aligned} \right\} \quad (12)$$

As shown above, the final differential system is controlled by several physical parameters, whose characteristics are well specified in Table 4.

From an engineering point of view, the strengths of the frictional drag force and heat transfer rate can be quantified locally at the Riga pattern through the following reduced forms of skin friction factor C_f and Nusselt number Nu :

$$C_f = -J_1 S''(0) \quad (13)$$

$$Nu = -J_4 H'(0) \quad (14)$$

Accordingly, we get the following simplified differential system:

Table 3 Adopted similarity transformations.

Quantities	Transformations: $\left\{ \eta = \sqrt{\frac{\rho_{bf}^s}{\mu_{bf}}}, S'(\eta) = \frac{u}{U_w}, S(\eta) = -\sqrt{\frac{\rho_{bf}^s}{\mu_{bf}}}v, H(\eta) = \frac{T-T_\infty}{\Delta T}, M(\eta) = \frac{C}{C_\infty} \right\}$			
	Partial derivatives of $\{u, v, T, C\}$ w.r.t. x and y			
u	$\frac{\partial u}{\partial x} = sS'(\eta)$	$\frac{\partial u}{\partial y} = U_w \sqrt{\frac{\rho_{bf}^s}{\mu_{bf}}} S'(\eta)$	$\frac{\partial^2 u}{\partial x^2} = 0$	$\frac{\partial^2 u}{\partial y^2} = \frac{U_w \rho_{bf}^s}{\mu_{bf}} S'''(\eta)$
v	$\frac{\partial v}{\partial x} = 0$	$\frac{\partial v}{\partial y} = -sS'(\eta)$	$\frac{\partial^2 v}{\partial x^2} = 0$	$\frac{\partial^2 v}{\partial y^2} = -s \sqrt{\frac{\rho_{bf}^s}{\mu_{bf}}} S''(\eta)$
T	$\frac{\partial T}{\partial x} = 0$	$\frac{\partial T}{\partial y} = \Delta T \sqrt{\frac{\rho_{bf}^s}{\mu_{bf}}} H'(\eta)$	$\frac{\partial^2 T}{\partial x^2} = 0$	$\frac{\partial^2 T}{\partial y^2} = \frac{\Delta T \rho_{bf}^s}{\mu_{bf}} H''(\eta)$
C	$\frac{\partial C}{\partial x} = 0$	$\frac{\partial C}{\partial y} = C_\infty \sqrt{\frac{\rho_{bf}^s}{\mu_{bf}}} M'(\eta)$	$\frac{\partial^2 C}{\partial x^2} = 0$	$\frac{\partial^2 C}{\partial y^2} = \frac{C_\infty \rho_{bf}^s}{\mu_{bf}} M''(\eta)$

Table 4 Involved flow parameters with their expressions and reference values.

Parameters	Expressions	Default Values	Ranges
Darcy porosity parameter	$\lambda = \frac{\mu_{bf}}{s\rho_{bf}K}$	5	$5 \leq \lambda \leq 8$
Forchheimer porosity parameter	$Fr = \frac{C_0}{\sqrt{K}}$	5	$5 \leq Fr \leq 20$
Geometrical parameter	$\kappa = \frac{\pi}{a_0} \sqrt{\frac{\mu_{bf}}{\rho_{bf}^s}}$	5	$\kappa = 5$
Hartmann number	$Ha = \frac{\pi j_0 M_0}{8s^2 \rho_{bf}}$	0.5	$0 \leq Ha \leq 1.5$
Nanoparticles' volume fraction	$\phi = \frac{V_{np}}{V_{bf} + V_{np}}$	0.025	$2.5\% \leq \phi \leq 10\%$
Prandtl number	$Pr = \frac{\mu_{bf}(C_p)_{bf}}{k_{bf}}$	6.0673898858	$Pr = 6.0673898858$
Biot number	$Bi = \frac{h}{k_{bf}} \sqrt{\frac{\mu_{bf}}{\rho_{bf}^s}}$	5	$2 \leq Bi \leq 5$
Thermophoresis parameter	$Nt = \frac{(\rho C_p)_{np} D_T \Delta T}{(C_p)_{bf} \mu_{bf} T_\infty}$	0.1	$0.1 \leq Nt \leq 0.4$
Brownian motion parameter	$Nb = \frac{(\rho C_p)_{np} D_B C_\infty}{(C_p)_{bf} \mu_{bf} \phi C}$	0.1	$0.1 \leq Nb \leq 0.4$
Schmidt number	$Sc = \frac{\mu_{bf}}{\rho_{bf} D_B}$	10	$10 \leq Sc \leq 25$

1.2. Methodology of solution with multiple validations

Due to the mathematical complexity of the nanofluid flow problem under consideration, the resulting nonlinear coupled differential system (S) shown in Eq. (12) is solved properly in Matlab software with the help of an efficient hybrid numerical algorithm GDQM - NRT built based on accurate differential quadrature schemes permitting a unidirectional spatial discretization of the derived governing ODEs on Gauss-

Lobatto grid points $\left\{ \eta_i = \frac{\eta_\infty}{2} - \frac{\eta_\infty}{2} \cos\left(\frac{\pi(i-1)}{N-1}\right), \text{ where } 1 \leq i \leq N \right\}$ [59]. These nodal points are distributed non-uniformly throughout the computational domain $I = [\eta_1, \eta_N] = [0, \eta_\infty]$. Here, the symbol N reflects the number of Gauss-Lobatto collocation points. After a successful differential quadrature discretization, the developed boundary value problem is converted into the following nonlinear coupled algebraic system:

$$\left(\bar{S} \right) : \left\{ \begin{array}{l} S(\eta_i) = 0, \sum_{j=1}^{j=N} P_{ij} S(\eta_j) = 1, \text{ when } i = 1, \\ \sum_{j=1}^{j=N} R_{ij} S(\eta_j) - \lambda \sum_{j=1}^{j=N} P_{ij} S(\eta_j) + \frac{j_2}{j_1} \left[\begin{array}{cc} S(\eta_i) & \sum_{j=1}^{j=N} P_{ij} S(\eta_j) \\ (1 + Fr) \sum_{j=1}^{j=N} P_{ij} S(\eta_j) & \sum_{j=1}^{j=N} Q_{ij} S(\eta_j) \end{array} \right] + \frac{Ha}{j_1} e^{(-\kappa \eta_i)} = 0, \text{ when } i \neq \{1, 2, N\}, \\ \sum_{j=1}^{j=N} P_{ij} S(\eta_j) = 0, \text{ when } i = N, \\ \sum_{j=1}^{j=N} P_{ij} H(\eta_j) = \frac{Bi}{j_4} [H(\eta_i) - 1], \text{ when } i = 1, \\ \sum_{j=1}^{j=N} Q_{ij} H(\eta_j) + \frac{Pr}{j_4} \left[J_3 S(\eta_i) + Nb \sum_{j=1}^{j=N} P_{ij} M(\eta_j) + Nt \sum_{j=1}^{j=N} P_{ij} H(\eta_j) \right] \sum_{j=1}^{j=N} P_{ij} H(\eta_j) = 0, \text{ when } i \neq \{1, N\}, \\ H(\eta_i) = 0, \text{ when } i = N, \\ \sum_{j=1}^{j=N} P_{ij} M(\eta_j) + \frac{Nt}{Nb} \sum_{j=1}^{j=N} P_{ij} H(\eta_j) = 0, \text{ when } i = 1, \\ \sum_{j=1}^{j=N} Q_{ij} M(\eta_j) + \frac{Nt}{Nb} \sum_{j=1}^{j=N} Q_{ij} H(\eta_j) + Sc S(\eta_i) \sum_{j=1}^{j=N} P_{ij} M(\eta_j) = 0, \text{ when } i \neq \{1, N\}, \\ M(\eta_i) = 1, \text{ when } i = N \end{array} \right. \quad (15)$$

Table 5 Multiple validations of GDQM - NRT results.

Nt	$\{J_1 = J_2 = J_3 = J_4 = 1, Ha = \kappa_1 = \lambda = Fr = 0, Bi \rightarrow \infty, Nb = 0.1, Sc = 10, \eta_\infty = 15, N = 70\}$		
	Sources	$-H'(0)$	
		Pr = 6.2	Pr = 14.2
0.1	Ishfaq et al. [71]	1.6198	2.4835
	Wakif et al. [72]	1.61980791	2.48355126
	Shah et al. [73]	1.6198079185	2.4835512644
	Present Results	1.6198079185	2.4835512644
	E	4.53×10^{-22}	4.59×10^{-22}
0.2	Ishfaq et al. [71]	1.4749	2.1815
	Wakif et al. [72]	1.47492523	2.18148324
	Shah et al. [73]	1.4749252363	2.1814832490
	Present Results	1.4749252363	2.1814832490
	E	4.05×10^{-22}	1.35×10^{-22}
0.3	Ishfaq et al. [71]	1.3381	1.8959
	Wakif et al. [72]	1.33812561	1.89589112
	Shah et al. [73]	1.338125615	1.895891266
	Present Results	1.338125615	1.895891266
	E	2.81×10^{-22}	2.76×10^{-22}
0.4	Ishfaq et al. [71]	1.2110	1.6371
	Wakif et al. [72]	1.21099539	1.63719091
	Shah et al. [73]	1.2109953930	1.6371909195
	Present Results	1.2109953931	1.6371909196
	E	5.54×10^{-22}	1.09×10^{-21}

According to Wakif et al. [60,61], the modified weighting differentiation coefficients $\{P_{ij}, Q_{ij}, R_{ij}\}$ can be written as:

$$\left\{ P_{ij} = \frac{\prod_{l=1, l \neq i}^{l=N} \left(\frac{\eta_{lc} - \eta_{lc}}{\eta_{lc} - \eta_{lc}} \right)}{\eta_{\infty} \left(\frac{\eta_{lc} - \eta_{lc}}{\eta_{\infty} - \eta_{\infty}} \right) \prod_{l=1, l \neq j}^{l=N} \left(\frac{\eta_{lc} - \eta_{lc}}{\eta_{\infty} - \eta_{\infty}} \right)}, \text{for } i \neq j \text{ and } P_{ij} = - \sum_{l=1, l \neq i}^{l=N} P_{lp}, \text{for } i = j \right\}, \tag{16}$$

$$\left\{ Q_{ij} = \frac{2}{\eta_{\infty}^2} \left(P_{ij} P_{ij} - \frac{P_{ij}}{\left(\frac{\eta_{lc} - \eta_{lc}}{\eta_{\infty} - \eta_{\infty}} \right)} \right), \text{for } i \neq j \text{ and } Q_{ij} = - \sum_{l=1, l \neq i}^{l=N} Q_{lp}, \text{for } i = j \right\}, \tag{17}$$

$$\left\{ R_{ij} = \frac{3}{\eta_{\infty}^3} \left(Q_{ij} P_{ij} - \frac{Q_{ij}}{\left(\frac{\eta_{lc} - \eta_{lc}}{\eta_{\infty} - \eta_{\infty}} \right)} \right), \text{for } i \neq j \text{ and } R_{ij} = - \sum_{l=1, l \neq i}^{l=N} R_{lp}, \text{for } i = j \right\}. \tag{18}$$

By invoking a robust Newton-Raphson algorithm, the gigantic algebraic system (\bar{S}) can be solved iteratively after selecting a sufficient number N of collocation points. For the sake of brevity, we focus herein only on the practical use of GDQM - NRT [61–68] as a powerful numerical procedure that can be utilized advantageously in several engineering studies as discussed comprehensively in the informative books of Shu et al. [69,70]. Concerning the authentication of the adopted methodology, extensive comparing tests of GDQM - NRT findings firstly with those published recently in well-reputed journals and secondly with those computed supplementary using RKFM - ST as seen in Table 5 and Table 6.

As expected, the aforesaid tabular illustrations show the existence of a higher order of agreement between the tabular datasets, which proves that the utilized numerical algorithm

Table 6 Comparison between RKFM-ST and GDQM - NRT results.

λ	$\{J_1 = J_2 = J_3 = J_4 = 1, Ha = \kappa_1 = 0, Fr = Bi = 5, Pr = 7, N_T = 0.2, N_B = 0.1, Sc = 2, \eta_\infty = 5, N = 70\}$			
	Methods	$-S''(0)$	$-H'(0)$	$M'(0)$
5	RKFM-ST*	3.0522229885	1.0991669584	2.1983339168
	GDQM-NRT*	3.0522229885	1.0991669584	2.1983339168
	E	5.14×10^{-21}		
10	RKFM-ST*	3.7845369473	1.0041599096	2.0083198193
	GDQM-NRT*	3.7845369472	1.0041599097	2.0083198193
	E	6.58×10^{-20}		
15	RKFM-ST*	4.3960961975	0.9310141579	1.8620283159
	GDQM-NRT*	4.3960961975	0.9310141579	1.8620283159
	E	1.49×10^{-20}		

RKFM-ST*: Runge-Kutta-Fehlberg Method- Shooting Technique.

GDQM-NRT*: Generalized Differential Quadrature Method- Newton-Raphson Technique.

GDQM - NRT can provide reliable results after p successive iterations with a feeble absolute accuracy ΔE and small total square residual error E (i.e., $\Delta E 10^{-10}$ and $E 10^{-22} - 10^{-19}$) when dividing the continuous domain I into sixty-nine irregular subdomains $I_i = [\eta_i, \eta_{i+1}]$ (i.e., $1 \leq i \leq N - 1$), such that:

$$I = \bigcup_{i=1}^{i=N-1} I_i, \tag{19}$$

$$\Delta E = \text{Max} \left\{ \left| S''_{p+1}(0) - S''_p(0) \right|, \left| H'_{p+1}(0) - H'_p(0) \right|, \left| M'_{p+1}(0) - M'_p(0) \right| \right\}, \tag{20}$$

$$E = E_S + E_H + E_M,$$

$$\Delta E = \text{Max} \left\{ \left| S''_{p+1}(0) - S''_p(0) \right|, \left| H'_{p+1}(0) - H'_p(0) \right|, \left| M'_{p+1}(0) - M'_p(0) \right| \right\}, \tag{21}$$

$$E_S = \int_{\eta=0}^{\eta=\eta_\infty} \left[S'''(\eta) - \lambda S'(\eta) + \frac{J_2}{J_1} \left| \frac{S(\eta)}{(1+Fr)S'(\eta)} \frac{S'(\eta)}{S''(\eta)} \right| + \frac{Ha}{J_1} e^{(-\kappa\eta)} \right]^2 d\eta, \tag{22}$$

$$E_H = \int_{\eta=0}^{\eta=\eta_\infty} \left\{ H''(\eta) + \frac{Pr}{J_4} [J_3 S(\eta) + Nb M'(\eta) + Nt H'(\eta)] H'(\eta) \right\}^2 d\eta, \tag{23}$$

$$E_M = \int_{\eta=0}^{\eta=\eta_\infty} \left[M''(\eta) + \frac{Nt}{Nb} H''(\eta) + Sc S(\eta) M'(\eta) \right]^2 d\eta. \tag{24}$$

2. Results and discussion

In light of the core objectives of the present investigation and the aforementioned computational considerations (i.e., accuracy, convergence criterion, validation), several clipped graphical illustrations are drawn noticeably in Figs. 2-20 under a perfect computational situation for the technical parameters

$\{\eta_\infty, N\}$ (e.g., $(\eta_\infty, N) = (10, 200)$) to produce admissible smooth curves and provide satisfactory answers to the remaining researcher questions via the parametric representations $\{S'(\eta), H(\eta), M(\eta), C_f, Nu\}$ reflecting the hydrothermal and mass aspects of the scrutinized non-homogeneous flow problem. These graphical displays are outlined for different values of λ – Darcy porosity parameter, Fr – Forchheimer porosity parameter, Ha – Hartmann number, ϕ – Nanoparticles’ volume fraction, Bi – Biot number, Nt – Thermophoresis parameter, Nb – Brownian motion parameter, and Sc – Schmidt number, which are varied in the vicinity of their defaults values

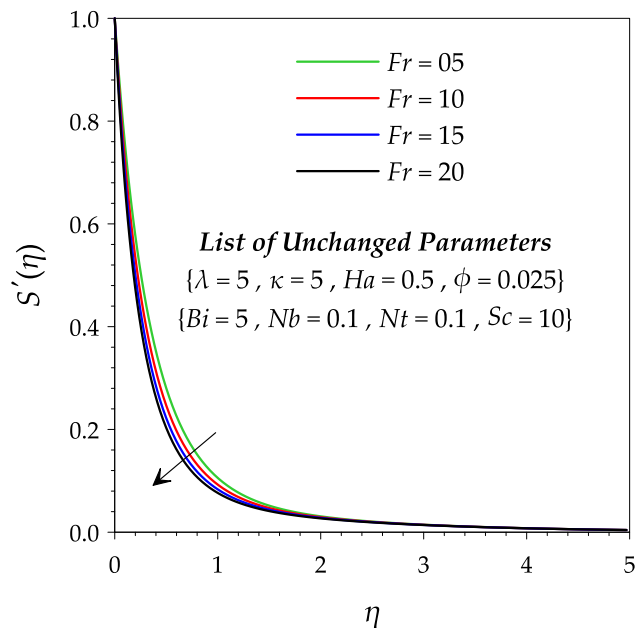


Fig. 3 Dynamical influence of Fr on $S'(\eta)$.

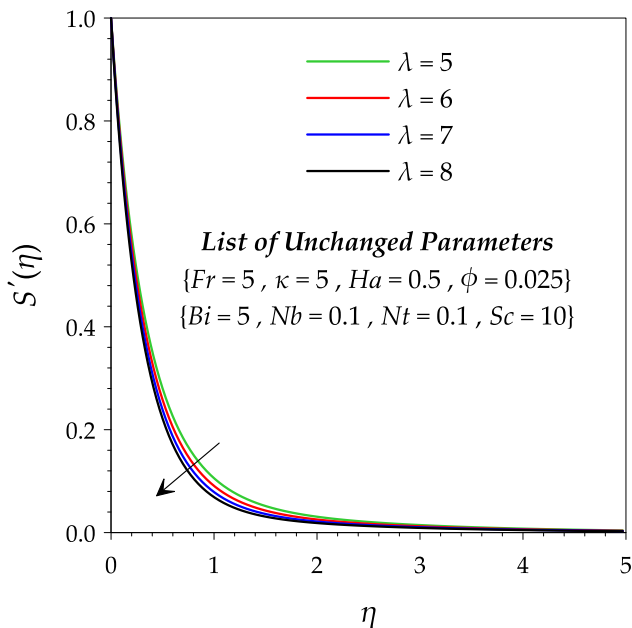


Fig. 2 Dynamical influence of λ on $S'(\eta)$.

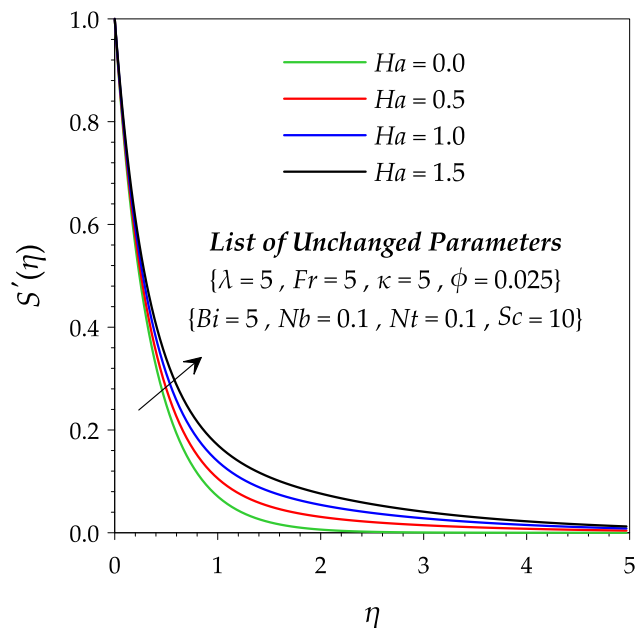


Fig. 4 Dynamical influence of Ha on $S'(\eta)$.

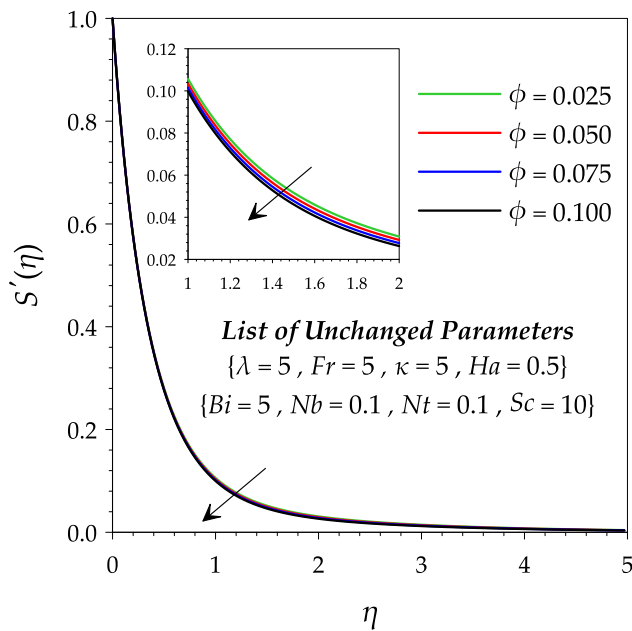


Fig. 5 Dynamical influence of ϕ on $S'(\eta)$.

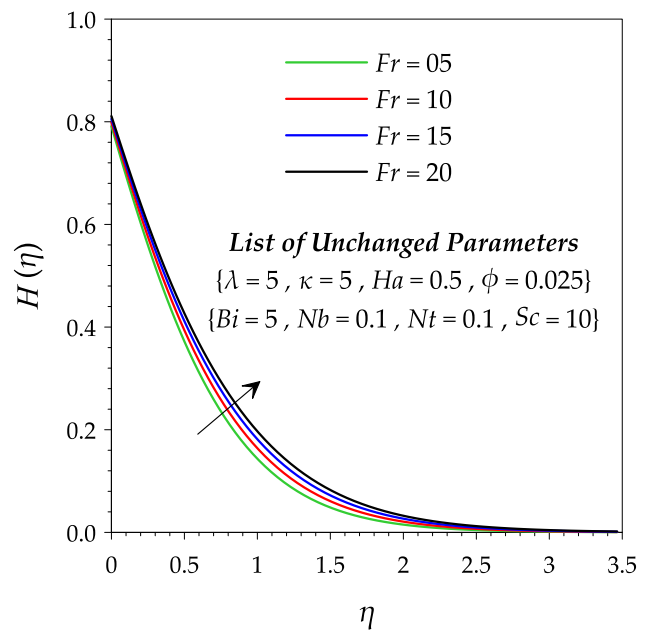


Fig. 7 Thermal impact of Fr on $H(\eta)$.

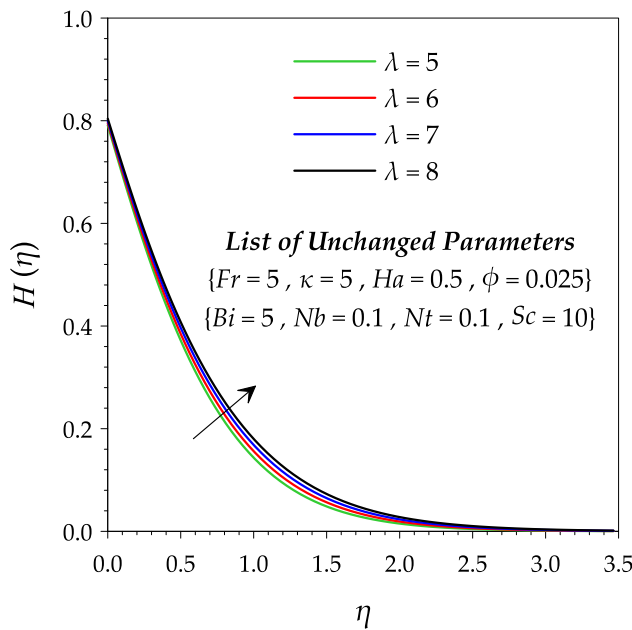


Fig. 6 Thermal impact of λ on $H(\eta)$.

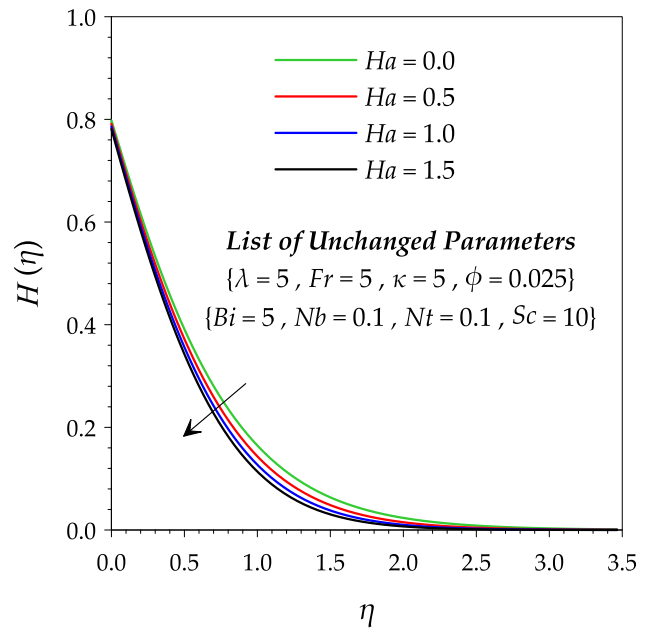


Fig. 8 Thermal impact of Ha on $H(\eta)$.

enlisted in Table 4. However, the dimensionless factors κ – Geometrical parameter and Pr – Prandtl number are kept constant in this examination at $\kappa = 5$ and $Pr = 6.0673898858$ (i.e., Prandtl value for pure water at the thermal reference state, which is assessed herein from the data of Table 1). A pre-analysis of the generated GDQM-NRT datasets depicts the influences of several parametric factors on the computed dimensionless quantities $S'(\eta)$ – Axial velocity, $H(\eta)$ – Temperature, $M(\eta)$ – Nanoparticles’ molar concentration, C_f – Skin friction factor, and Nu – Nusselt number distinguishing the steady motion of alumina-based pure water nanofluid over

a horizontal active Riga plate in a Darcy-Forchheimer porous medium.

Dynamically, the noteworthy impacts of λ – Darcy porosity parameter, Fr – Forchheimer porosity parameter, Ha – Hartmann number, and ϕ – Nanoparticles’ volume fraction on the nanofluid motion are profiled respectively in terms of the velocity function $S'(\eta)$ as shown in Figs. 2-5. Due to the porosity trend of the nanofluidic medium, the nonlinear porous structure of the existing internal solid matrix exerts opposing Darcy’s and Forchheimer’s forces on the nanofluid motion. For this reason, the velocity function $S'(\eta)$ and its cor-

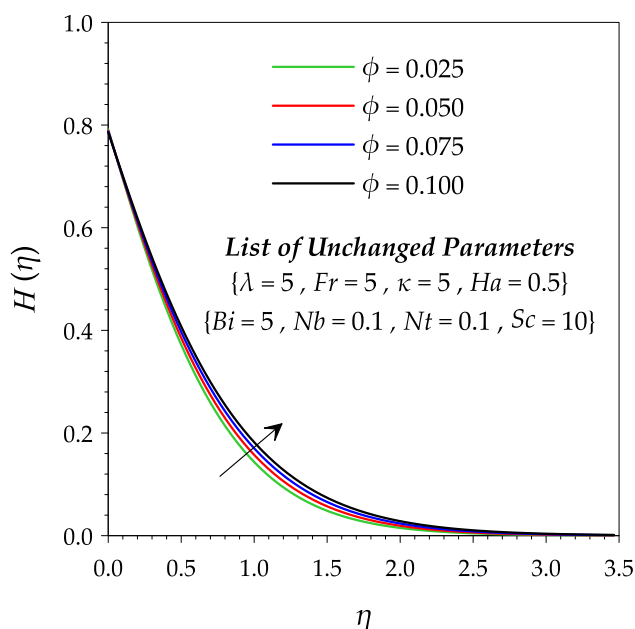


Fig. 9 Thermal impact of ϕ on $H(\eta)$.

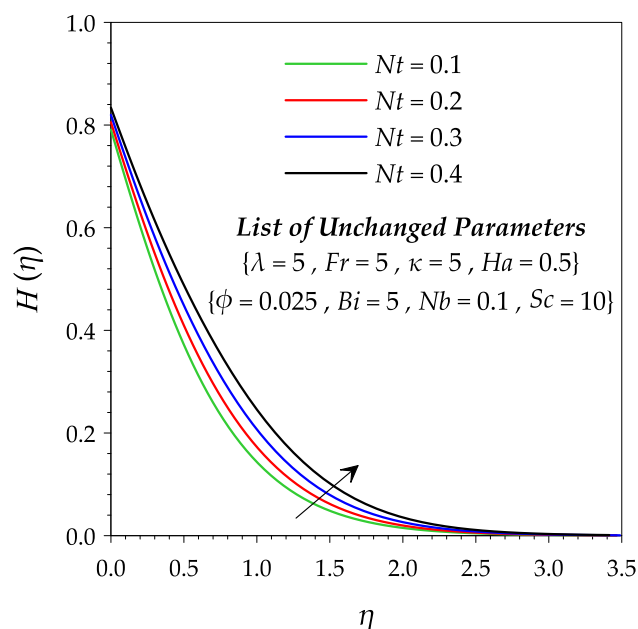


Fig. 11 Thermal impact of Nt on $H(\eta)$.

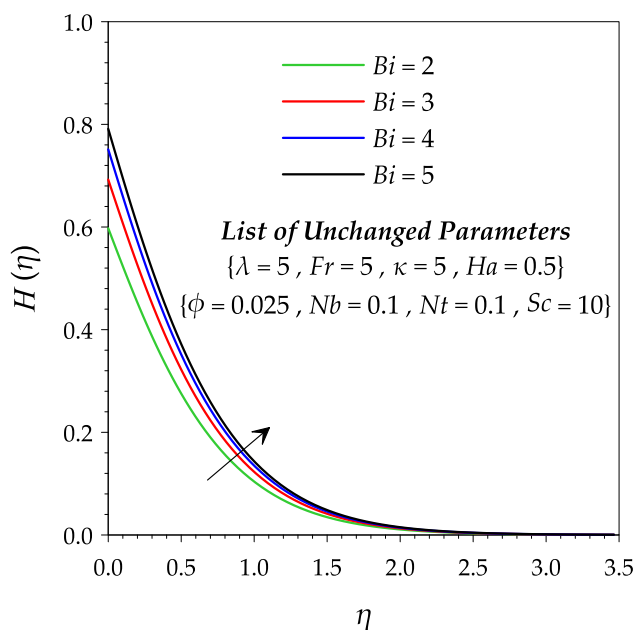


Fig. 10 Thermal impact of Bi on $H(\eta)$.

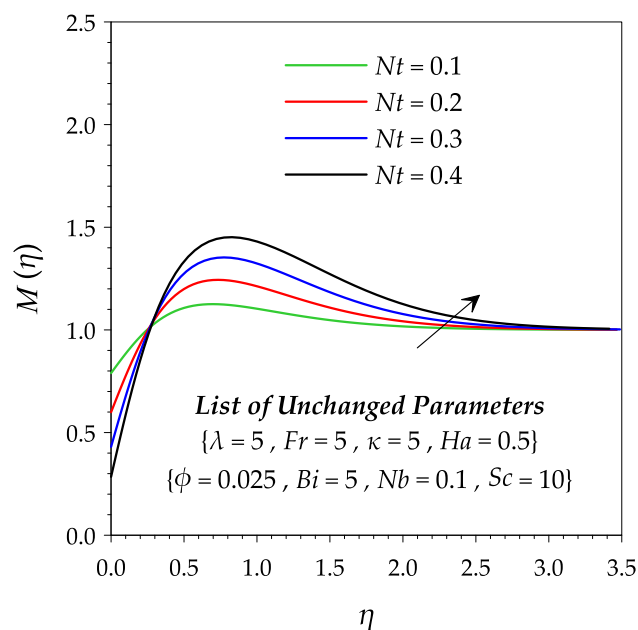


Fig. 12 Mass impression of Nt on $M(\eta)$.

responding momentum boundary layer thickness show a declining aspect, when the magnitudes of λ – Darcy porosity parameter and Fr – Forchheimer porosity are augmented progressively as seen in Fig. 2 and Fig. 3. On the contrary, Fig. 4 reveals that the velocity function $S'(\eta)$ exhibit an escalating trend with the higher values of Ha – Hartmann number. This observation is enormously true because the magnets and electrodes of the electromagnetic actuator (i.e., Riga pattern) are arranged in such a way that the induced Lorentz forces play a driven dynamical role during the motion of the studied electrically conducting nanofluid. Similarly, Fig. 5 proves that the velocity profile $S'(\eta)$ is a slightly falling function with the

growing values of ϕ – Nanoparticles' volume fraction. Accordingly, the nanoparticles' loading process of alumina into a purely aquatic fluidic medium diminishes somewhat the rheological fluidity tendency of the resulting biphasic mixture due to an improvement in its effective viscosity, which leads to a dynamical slowing down influence on the nanofluid motion.

From another point of view, the thermal impressions of λ – Darcy porosity parameter, Fr – Forchheimer porosity parameter, Ha – Hartmann number, ϕ – Nanoparticles' volume fraction, Bi – Biot number, and Nt – Thermophoresis parameter are sketched respectively in terms of the temperature function

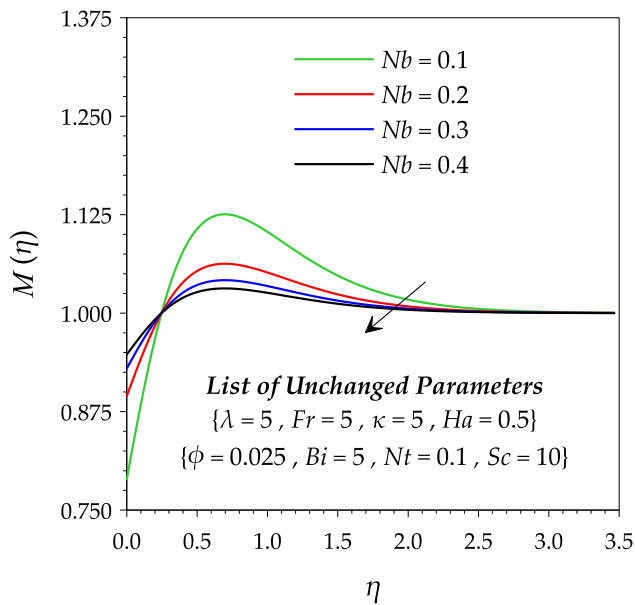


Fig. 13 Mass impression of Nb on $M(\eta)$.

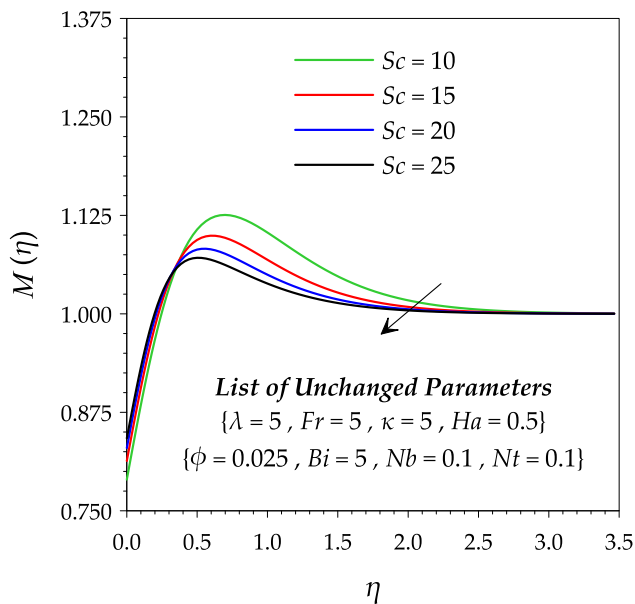


Fig. 14 Mass impression of Sc on $M(\eta)$.

$H(\eta)$ as portrayed in Figs. 6-11. As a result of the resistive demeanor of Darcy’s and Forchheimer’s forces, a substantial amount of thermal energy is communicated to the nanofluidic medium due to the viscous frictional interaction between the nanofluid and the solid porous matrix. Consequently, the temperature function $H(\eta)$ and its associated thermal boundary layer thickness upsurge significantly with the strengthening values of λ – Darcy porosity parameter and Fr – Forchheimer porosity parameter as emphasized in Fig. 6 and Fig. 7. However, Fig. 8 ascertains that the driven electromagnetic aspect of Lorentz’s forces causes a cooling effect on the nanofluidic system throughout the thermal boundary layer region. Therefore, the temperature distribution $H(\eta)$ is a dropping function

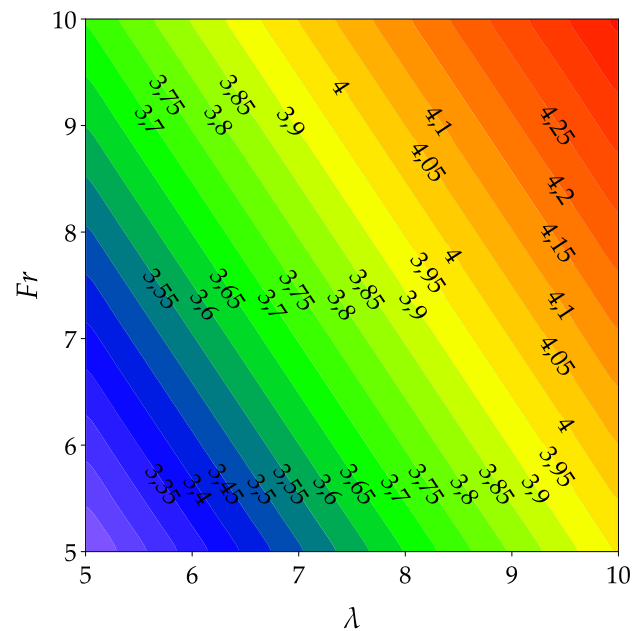


Fig. 15 Frictional sways of λ and Fr on C_f . $\{\kappa = 5, Ha = 0.5, \phi = 0.025, Bi = 5, Nb = 0.1, Nt = 0.1, Sc = 10\}$

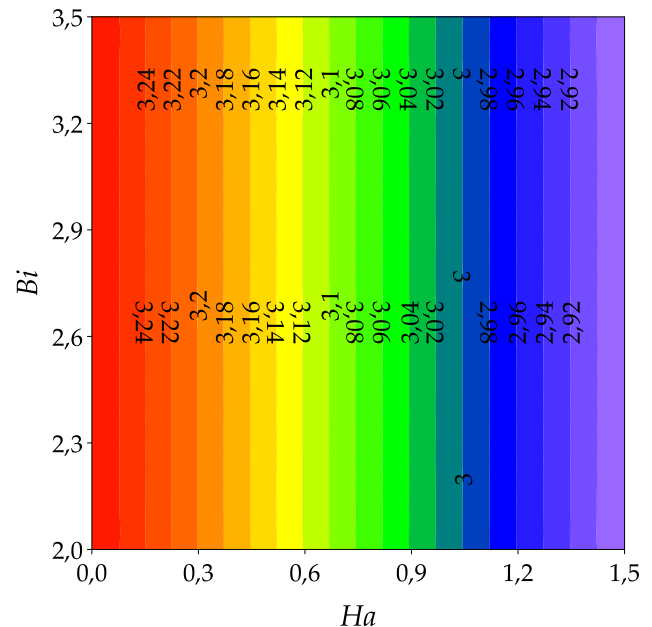


Fig. 16 Frictional sways of Ha and Bi on C_f . $\{\lambda = 5, Fr = 5, \kappa = 5, \phi = 0.025, Nb = 0.1, Nt = 0.1, Sc = 10\}$

of Ha – Hartmann number. A prominent thermal enhancement is evidenced in Fig. 9 with the nanoparticles loading of alumina into the hosting fluidic medium, in which the temperature function $H(\eta)$ exhibits an impeccable raise with the advancing values of ϕ – Nanoparticles’ volume fraction. Indeed, this enrichment is due predominantly to the increasing relationship between the effective thermal conductivity k_{nf} of the nanofluidic medium and the volume fraction ϕ of alumina nanoparticles. Physically, the higher values of Bi – Biot num-

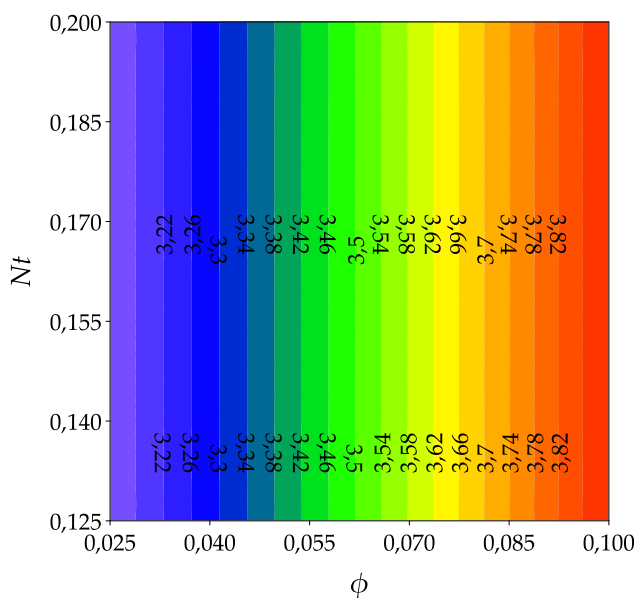


Fig. 17 Frictional sways of ϕ and Nt on C_f . $\{\lambda = 5, Fr = 5, \kappa = 5, Ha = 0.5, Bi = 5, Nb = 0.1, Sc = 10\}$

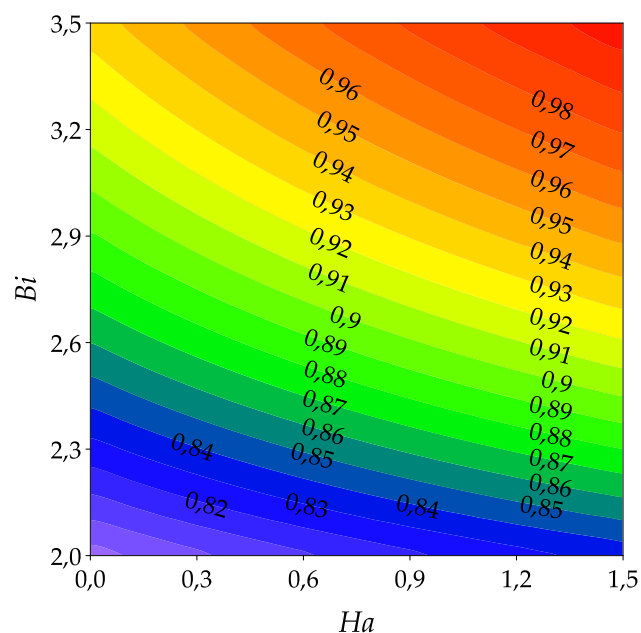


Fig. 19 Energetical effects of Ha and Bi on Nu . $\{\lambda = 5, Fr = 5, \kappa = 5, \phi = 0.025, Nb = 0.1, Nt = 0.1, Sc = 10\}$

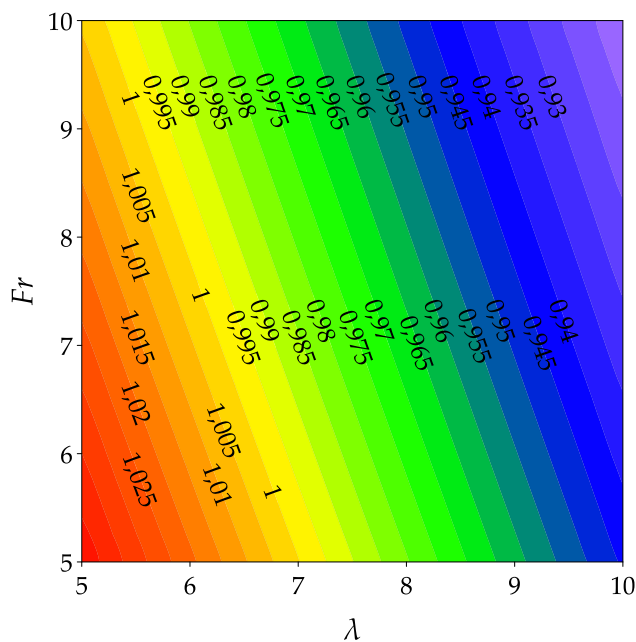


Fig. 18 Energetical effects of λ and Fr on Nu . $\{\kappa = 5, Ha = 0.5, \phi = 0.025, Bi = 5, Nb = 0.1, Nt = 0.1, Sc = 10\}$

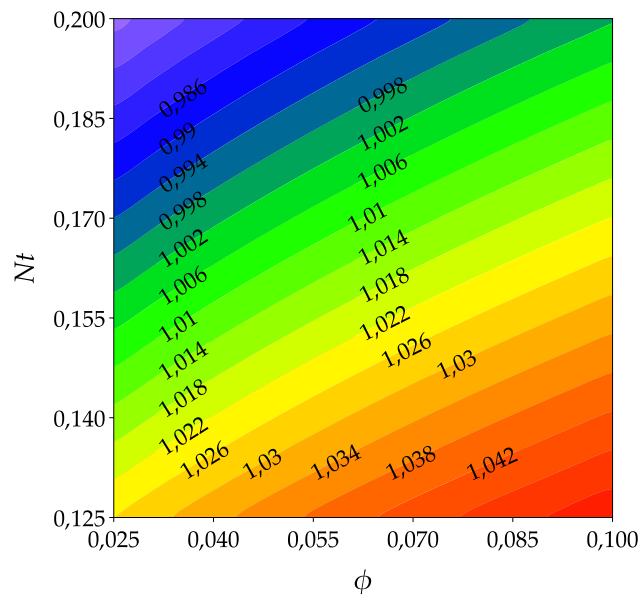


Fig. 20 Energetical effects of ϕ and Nt on Nu . $\{\lambda = 5, Fr = 5, \kappa = 5, Ha = 0.5, Bi = 5, Nb = 0.1, Sc = 10\}$

ber feebleness considerably the convective thermal resistance between the external heating fluid and the contact surface (i.e., Riga plate). Whilst, the bigger values of Nt – Thermophoresis reinforce the mechanical effect of thermophoretic forces on alumina nanoparticles by supporting the upwards thermo-migration of alumina nanoparticles from the hot region to the cold zone within the nanofluidic medium. Therefore, an extensive heightening in the temperature distribution $H(\eta)$ throughout the whole thermal boundary layer

region can be reached straightforwardly just by adjusting increasingly the magnitudes of Bi – Biot number and Nt – Thermophoresis parameter as demonstrated in Fig. 10 and Fig. 11.

Nanoparticles’ molar concentration.

Specifically, the crucial mass sways of Nt – Thermophoresis parameter, Nb – Brownian motion parameter, and Sc – Schmidt number on the nanoparticles’ molar concentration function $M(\eta)$ are well elucidated in Figs. 12–14. Generally, it is

Table 7 Frictional and energetical behaviors of the parameters $\{\lambda, Fr, \phi, Ha, Bi, Nt\}$.

Parameters	C_f		Nu	
	Descriptions	Surface Viscous Drag Forces	Descriptions	Surface Heat Transfer Rates
λ	Rising function	Strengthening impact	Falling function	Dropping effect
Fr	Rising function	Strengthening impact	Falling function	Dropping effect
ϕ	Rising function	Strengthening impact	Rising function	Enhancing effect
Ha	Falling function	Weakening influence	Rising function	Enhancing effect
Bi	No influence	No influence	Rising function	Enhancing effect
Nt	No influence	No influence	Falling function	Dropping effect

proved that the governing parameters $\{Nt, Nb, Sc\}$ disclose a dual role during the occurrence of mass transport phenomenon throughout the concentration boundary region. In this respect, Fig. 12 ascertains that the elevating values of Nt —Thermophoresis parameter promote strongly the upward thermomigration of alumina nanoparticles to reach a top-heavy configuration of nanoparticles. As a remarkable result of the strengthening action on the magnitude of Nt —Thermophoresis parameter, the nanoparticles’ molar concentration function $M(\eta)$ decreases noticeably near the hot surface (i.e., Riga plate) to get a prominent rise away from it. On the contrary, Fig. 13 shows that the bottom-heavy distribution of nanoparticles (i.e., the downward migration of alumina nanoparticles from the concentrate region to the dilute zone) can be achieved effectively as a result of the intensifying values of Nb —Brownian motion parameter. Likewise, the curves of Fig. 14 reflect undoubtedly the deteriorating behavior of Sc —Schmidt number on the concentration boundary layer region with a reinforcement in the bottom-heavy distribution of nanoparticles.

Sequel the above finding, Figs. 15-20 illuminates the frictional and energetical influences of the embedded parameters $\{\lambda, Fr, \phi, Ha, Bi, Nt\}$ on the engineering quantity of interest $\{C_f, Nu\}$, whose descriptions are well enlightened in Table 7.

2.1. Concluding remarks

The foremost hydrothermal aspects of non-Darcian convective nanofluid flows over a horizontal active electromagnetic actuator (i.e., Riga device) have been explored numerically for alumina-based pure water nanofluids by considering the non-homogeneous nanofluid model and passive control approach. Among the most important reached upshots, we can state exclusively the following conclusions:

1. The nanoparticles’ loading process has an enhancing thermal effect and a slowing down impact.
2. The advanced values of the porosity factors decline the nanofluid velocity and rise the thermal profile.
3. The induced Lorentz forces exhibit a cooling effect with a driven dynamical role.
4. The convective heating process and the thermophoresis mechanism improve significantly the nanofluid temperature.
5. The thermophoresis mechanism reinforces the top-heavy configuration of nanoparticles, whereas the Brownian motion promotes the bottom-heavy distribution of nanoparticles.

6. The higher Schmidt’s numbers weaken the thermomigration of nanoparticles.
7. The used electromagnetic actuator minimizes the strength of surface viscous drag forces and enhances the surface heat transfer rate.
8. The porosity factors have a strengthening impact on the surface viscous drag forces and a reducing effect on the surface heat transfer rate.
9. The thermophoresis mechanism diminishes the surface heat transfer rate.
10. The convective heating and nanoparticles’ loading processes enhance the surface heat transfer rate.

Declaration of Competing Interest

The authors declare that they have no known competing financial interests or personal relationships that could have appeared to influence the work reported in this paper.

References

- [1] H. Babar, H.M. Ali, Towards hybrid nanofluids: preparation, thermophysical properties, applications, and challenges, *J. Mol. Liq.* 281 (2019) 598–633, <https://doi.org/10.1016/j.molliq.2019.02.102>.
- [2] H. Babar, H.M. Ali, Airfoil shaped pin-fin heat sink: potential evaluation of ferric oxide and titania nanofluids, *Energy Convers. Manag.* 202 (2019), <https://doi.org/10.1016/j.enconman.2019.112194> 112194.
- [3] T.R. Shah, H.M. Ali, Applications of hybrid nanofluids in solar energy, practical limitations and challenges: a critical review, *Sol. Energy.* 183 (2019) 173–203, <https://doi.org/10.1016/j.solener.2019.03.012>.
- [4] C. Li, H.M. Ali, Enhanced heat transfer mechanism of nanofluid MQL Cooling Grinding, Hershey, PA: IGI Global (2020), <https://doi.org/10.4018/978-1-7998-1546-4>.
- [5] M.M. Bhatti, M.B. Arain, A. Zeeshan, R. Ellahi, M.H. Doranehgard, Swimming of Gyrotactic Microorganism in MHD Williamson nanofluid flow between rotating circular plates embedded in porous medium: application of thermal energy storage, *J. Energy Storage.* 45 (2022), <https://doi.org/10.1016/j.est.2021.103511> 103511.
- [6] M.M. Bhatti, R. Ellahi, M. Hossein Doranehgard, Numerical study on the hybrid nanofluid (Co3O4-Go/H2O) flow over a circular elastic surface with non-Darcy medium: application in solar energy, *J. Mol. Liq.* 361 (2022), <https://doi.org/10.1016/j.molliq.2022.119655> 119655.
- [7] M.M. Rashidi, I. Mahariq, M. Alhuyi Nazari, O. Accouche, M. M. Bhatti, Comprehensive review on exergy analysis of shell and

- tube heat exchangers, *J. Therm. Anal. Calorim.* 147 (2022) 12301–12311, <https://doi.org/10.1007/s10973-022-11478-2>.
- [8] M.D. Ikram, M.A. Imran, Y.M. Chu, A. Akgül, MHD flow of a Newtonian fluid in symmetric channel with ABC fractional model containing hybrid nanoparticles, *Comb. Chem. High Throughput Screen.* 25 (2022) 1087–1102, <https://doi.org/10.2174/1386207324666210412122544>.
- [9] J. Buongiorno, D.C. Venerus, N. Prabhat, T. McKrell, J. Townsend, R. Christianson, Y.V. Tolmachev, P. Keblinski, L.-W. Hu, J.L. Alvarado, I.C. Bang, S.W. Bishnoi, M. Bonetti, F. Botz, A. Cecere, Y. Chang, G. Chen, H. Chen, S.J. Chung, M.K. Chyu, S.K. Das, R. Di Paola, Y. Ding, F. Dubois, G. Dzido, J. Eapen, W. Escher, D. Funfschilling, Q. Galand, J. Gao, P.E. Gharagozloo, K.E. Goodson, J.G. Gutierrez, H. Hong, M. Horton, K.S. Hwang, C.S. Iorio, S.P. Jang, A.B. Jarzebski, Y. Jiang, L. Jin, S. Kabelac, A. Kamath, M.A. Kedzierski, L.G. Kieng, C. Kim, J.-H. Kim, S. Kim, S.H. Lee, K.C. Leong, I. Manna, B. Michel, R. Ni, H.E. Patel, J. Philip, D. Poulidakos, C. Reynaud, R. Savino, P.K. Singh, P. Song, T. Sundararajan, E. Timofeeva, T. Triticak, A.N. Turanov, S. Van Vaerenbergh, D. Wen, S. Witharana, C. Yang, W.-H. Yeh, X.-Z. Zhao, S.-Q. Zhou, McKrell, A benchmark study on the thermal conductivity of nanofluids, *J. Appl. Phys.* 106 (9) (2009) 094312.
- [10] X. Li, F. Yuan, W. Tian, C. Dai, X. Yang, D. Wang, J. Du, W. Yu, H. Yuan, Heat transfer enhancement of nanofluids with non-spherical nanoparticles: a review, *Appl. Sci.* 12 (2022) 1–23, <https://doi.org/10.3390/app12094767>.
- [11] J. Wen, X. Li, H. Zhang, M. Chen, X. Wu, Enhancement of solar absorption performance using TiN@SiCw plasmonic nanofluids for effective photo-thermal conversion: Numerical and experimental investigation, *Renew. Energy.* 193 (2022) 1062–1073, <https://doi.org/10.1016/j.renene.2022.05.074>.
- [12] M. Javidan, A.J. Moghadam, Effective cooling of a photovoltaic module using jet-impingement array and nanofluid coolant, *Int. Commun. Heat Mass Transf.* 137 (2022), <https://doi.org/10.1016/j.icheatmasstransfer.2022.106310> 106310.
- [13] D. Maillet, A review of the models using the Cattaneo and Vernotte hyperbolic heat equation and their experimental validation, *Int. J. Therm. Sci.* 139 (2019) 424–432, <https://doi.org/10.1016/j.ijthermalsci.2019.02.021>.
- [14] G. Chen, Non-Fourier phonon heat conduction at the microscale and nanoscale, *Nat. Rev. Phys.* 3 (2021) 555–569, <https://doi.org/10.1038/s42254-021-00334-1>.
- [15] J.B.J. Fourier, G. Darboux, *Théorie analytique de la chaleur*, Didot Paris, 1822.
- [16] C. Cattaneo, *Sulla Conduzione del Calore*, *Atti Del Semin. Mat. e Fis. Dell'Universita.* 3 (1948) 83–101.
- [17] C.I. Christov, On frame indifferent formulation of the Maxwell-Cattaneo model of finite-speed heat conduction, *Mech. Res. Commun.* 36 (2009) 481–486, <https://doi.org/10.1016/j.mechrescom.2008.11.003>.
- [18] S. Bilal, M. Imtiaz Shah, N.Z. Khan, A. Akgül, K.S. Nisar, Onset about non-isothermal flow of Williamson liquid over exponential surface by computing numerical simulation in perspective of Cattaneo Christov heat flux theory, *Alexandria Eng. J.* 61 (2022) 6139–6150, <https://doi.org/10.1016/j.aej.2021.11.038>.
- [19] A. Shahzad, M. Imran, M. Tahir, S. Ali Khan, A. Akgül, S. Abdullaev, C. Park, H.Y. Zahran, I.S. Yahia, Brownian motion and thermophoretic diffusion impact on Darcy-Forchheimer flow of bioconvective micropolar nanofluid between double disks with Cattaneo-Christov heat flux, *Alexandria Eng. J.* 62 (2023) 1–15, <https://doi.org/10.1016/j.aej.2022.07.023>.
- [20] Z. Shah, E.O. Alzahrani, A. Dawar, W. Alghamdi, M. Zaka Ullah, Entropy generation in MHD second-grade nanofluid thin film flow containing CNTs with Cattaneo-Christov heat flux model past an unsteady stretching sheet, *Appl. Sci.* 10 (2020) 1–21, <https://doi.org/10.3390/app10082720>.
- [21] P. Ragupathi, N.A. Ahammad, A. Wakif, N.A. Shah, Y. Jeon, Exploration of multiple transfer phenomena within viscous fluid flows over a curved stretching sheet in the co-existence of gyrotactic micro-organisms and tiny particles, *Mathematics.* 10 (2022) 1–18, <https://doi.org/10.3390/math10214133>.
- [22] J. Buongiorno, Convective transport in nanofluids, *J. Heat Transfer.* 128 (2006) 240–250, <https://doi.org/10.1115/1.2150834>.
- [23] J. Sharma, A. Wakif, Comprehensive analyses of probable influencing factors responsible for the onset of convective instabilities in various viscous fluidic media involving metallic/non-metallic nanoparticles, *Waves in Random and Complex Media.* (2022) 1–20, <https://doi.org/10.1080/17455030.2022.2117878>.
- [24] M. Ramzan, H. Gul, S. Kadry, Y.M. Chu, Role of bioconvection in a three-dimensional tangent hyperbolic partially ionized magnetized nanofluid flow with Cattaneo-Christov heat flux and activation energy, *Int. Commun. Heat Mass Transf.* 120 (2021), <https://doi.org/10.1016/j.icheatmasstransfer.2020.104994> 104994.
- [25] U. Farooq, H. Waqas, M.I. Khan, S.U. Khan, Y.-M. Chu, S. Kadry, Thermally radioactive bioconvection flow of Carreau nanofluid with modified Cattaneo-Christov expressions and exponential space-based heat source, *Alexandria Eng. J.* 60 (2021) 3073–3086, <https://doi.org/10.1016/j.aej.2021.01.050>.
- [26] A. Hafeez, M. Khan, A. Ahmed, J. Ahmed, Features of Cattaneo-Christov double diffusion theory on the flow of non-Newtonian Oldroyd-B nanofluid with Joule heating, *Appl. Nanosci.* 12 (2022) 265–272, <https://doi.org/10.1007/s13204-020-01600-x>.
- [27] N.H. Hamad, A. Wakif, A. Alshehri, Towards the dynamics of a radiative-reactive magnetized viscoelastic nanofluid involving gyrotactic microorganisms and flowing over a vertical stretching sheet under multiple convective and stratification constraints, *Waves in Random and Complex Media.* (2022) 1–31, <https://doi.org/10.1080/17455030.2022.2100944>.
- [28] S. Rehman, R. Haq, Z.H. Khan, C. Lee, Entropy generation analysis for non-Newtonian nanofluid with zero normal flux of nanoparticles at the stretching surface, *J. Taiwan Inst. Chem. Eng.* 63 (2016) 226–235, <https://doi.org/10.1016/j.jtice.2016.03.006>.
- [29] P. Rana, M. Khurana, S. Srivastava, Linear stability analysis on the onset of MHD non-newtonian viscoelastic rotating nanofluid layer with heat generation, *AIP Conf. Proc.*, AIP Publishing (2017) 1–8, <https://doi.org/10.1063/1.5008709>.
- [30] P. Besthapu, R.U. Haq, S. Bandari, Q.M. Al-Mdallal, Thermal radiation and slip effects on MHD stagnation point flow of non-Newtonian nanofluid over a convective stretching surface, *Neural Comput. Appl.* 31 (2019) 207–217, <https://doi.org/10.1007/s00521-017-2992-x>.
- [31] R. Jawad, F. Mushayyda, M.-O. Fateh, M. b., Multiple slip effects on MHD non-Newtonian nanofluid flow over a nonlinear permeable elongated sheet: Numerical and statistical analysis, *Multidiscip. Model. Mater. Struct.* 15 (2019) 913–931, <https://doi.org/10.1108/MMMS-11-2018-0190>.
- [32] A. Hafeez, M. Khan, J. Ahmed, Stagnation point flow of radiative Oldroyd-B nanofluid over a rotating disk, *Comput. Methods Programs Biomed.* 191 (2020), <https://doi.org/10.1016/j.cmpb.2020.105342> 105342.
- [33] A. Raees, U. Farooq, M. Hussain, W.A. Khan, F.B. Farooq, Non-similar mixed convection analysis for magnetic flow of second-grade nanofluid over a vertically stretching sheet, *Commun. Theor. Phys.* 73 (2021) 65801, <https://doi.org/10.1088/1572-9494/abe932>.
- [34] A. Gaillitis, *On the possibility to reduce the hydrodynamic drag of a plate in an electrolyte*, *Appl. Magnetohydrodyn. Rep. Inst. Phys. Riga.* 13 (1961) 143–146.

- [35] E. Grinberg, On the determination of properties of some potential fields, *Applied Magnetohydrodynamics*, Appl. Magnetohydrodyn. Repub. Phys. Inst. Riga. 12 (1961) 147–154.
- [36] A. Wakif, A. Chamkha, I.L. Animasaun, M. Zaydan, H. Waqas, R. Sehaqui, Novel Physical Insights into the Thermodynamic Irreversibilities Within Dissipative EMHD Fluid Flows Past over a Moving Horizontal Riga Plate in the Coexistence of Wall Suction and Joule Heating Effects: A Comprehensive Numerical Investigation, *Arab. J. Sci. Eng.* 45 (2020) 9423–9438, <https://doi.org/10.1007/s13369-020-04757-3>.
- [37] G. Rasool, N.A. Shah, E.R. El-Zahar, A. Wakif, Numerical investigation of EMHD nanofluid flows over a convectively heated Riga pattern positioned horizontally in a Darcy-Forchheimer porous medium: application of passive control strategy and generalized transfer laws, *Waves in Random and Complex Media* (2022) 1–20, <https://doi.org/10.1080/17455030.2022.2074571>.
- [38] S. Abdal, I. Siddique, A.S. Alshomrani, F. Jarad, I.S. Ud Din, S. Afzal, Significance of chemical reaction with activation energy for Riga wedge flow of tangent hyperbolic nanofluids in the existence of heat source, *Case Stud. Therm. Eng.* 28 (2021), <https://doi.org/10.1016/j.csite.2021.101542> 101542.
- [39] M. Naveed, M. Imran, Z. Abbas, A. Nadeem, Analysis of entropy generation and Joule heating on curvilinear flow of thermally radiative viscous fluid due to an oscillation of curved Riga surface, *Int. J. Mod. Phys. C* 33 (2021) 2250087, <https://doi.org/10.1142/S0129183122500875>.
- [40] N. Abbas, S. Nadeem, M.Y. Malik, Theoretical study of micropolar hybrid nanofluid over Riga channel with slip conditions, *Phys. A Stat. Mech. Its Appl.* 551 (2020), <https://doi.org/10.1016/j.physa.2019.124083> 124083.
- [41] Z. Hussain, Z. Bashir, M.S. Anwar, Analysis of nanofluid flow subject to velocity slip and Joule heating over a nonlinear stretching Riga plate with varying thickness, *Waves in Random and Complex Media* (2022) 1–17, <https://doi.org/10.1080/17455030.2022.2124468>.
- [42] P. Ragupathi, T. Muhammad, S. Islam, A. Wakif, Application of Arrhenius kinetics on MHD radiative Von Kármán Casson nanofluid flow occurring in a Darcy-Forchheimer porous medium in the presence of an adjustable heat source, *Phys. Scr.* 96 (12) (2021) 125228.
- [43] A. Wakif, I.L. Animasaun, U. Khan, N.A. Shah, T. Thumma, Dynamics of radiative-reactive Walters-B fluid due to mixed convection conveying gyrotactic microorganisms, tiny particles experience haphazard motion, thermo-migration, and Lorentz force, *Phys. Scr.* 96 (12) (2021) 125239.
- [44] A.S. Sabu, A. Wakif, S. Areekara, A. Mathew, N.A. Shah, Significance of nanoparticles' shape and thermo-hydrodynamic slip constraints on MHD alumina-water nanofluid flows over a rotating heated disk: The passive control approach, *Int. Commun. Heat Mass Transf.* 129 (2021), <https://doi.org/10.1016/j.icheatmasstransfer.2021.105711> 105711.
- [45] M. Alghamdi, A. Wakif, T. Thumma, U. Khan, D. Baleanu, G. Rasool, Significance of variability in magnetic field strength and heat source on the radiative-convective motion of sodium alginate-based nanofluid within a Darcy-Brinkman porous structure bounded vertically by an irregular slender surface, *Case Stud. Therm. Eng.* 28 (2021), <https://doi.org/10.1016/j.csite.2021.101428> 101428.
- [46] A. Dawar, N.M. Said, S. Islam, Z. Shah, S.R. Mahmood, A. Wakif, A semi-analytical passive strategy to examine a magnetized heterogeneous mixture having sodium alginate liquid with alumina and copper nanomaterials near a convectively heated surface of a stretching curved geometry, *Int. Commun. Heat Mass Transf.* 139 (2022), <https://doi.org/10.1016/j.icheatmasstransfer.2022.106452> 106452.
- [47] E.A. Algehyne, A. Wakif, G. Rasool, A. Saeed, Z. Ghouli, Significance of Darcy-Forchheimer and Lorentz forces on radiative alumina-water nanofluid flows over a slippery curved geometry under multiple convective constraints: a renovated Buongiorno's model with validated thermophysical correlations, *Waves in Random and Complex Media* (2022) 1–30, <https://doi.org/10.1080/17455030.2022.2074570>.
- [48] A. Dawar, A. Wakif, A. Saeed, Z. Shah, T. Muhammad, P. Kumam, Significance of Lorentz forces on Jeffrey nanofluid flows over a convectively heated flat surface featured by multiple velocity slips and dual stretching constraint: a homotopy analysis approach, *J. Comput. Des. Eng.* 9 (2022) 564–582, <https://doi.org/10.1093/jcde/qwac019>.
- [49] A. Dawar, A. Wakif, T. Thumma, N.A. Shah, Towards a new MHD non-homogeneous convective nanofluid flow model for simulating a rotating inclined thin layer of sodium alginate-based Iron oxide exposed to incident solar energy, *Int. Commun. Heat Mass Transf.* 130 (2022), <https://doi.org/10.1016/j.icheatmasstransfer.2021.105800> 105800.
- [50] H. Schlichting, K. Gersten, *Boundary-layer theory*, Springer, Berlin, Heidelberg (2017), <https://doi.org/10.1007/978-3-662-52919-5>.
- [51] N.A. Shah, I.L. Animasaun, J.D. Chung, A. Wakif, F.I. Alao, C.S.K. Raju, Significance of nanoparticle's radius, heat flux due to concentration gradient, and mass flux due to temperature gradient: The case of Water conveying copper nanoparticles, *Sci. Rep.* 11 (2021) 1882, <https://doi.org/10.1038/s41598-021-81417-y>.
- [52] J. Li, Computational analysis of nanofluid flow in micro-channels with applications to micro-heat sinks and bio-MEMS. Ph.D. Thesis NC State University, Raleigh, NC, the United States, Raleigh, NC, United States. (2008).
- [53] K. Mehmood, S. Hussain, M. Sagheer, Numerical simulation of MHD mixed convection in alumina-water nanofluid filled square porous cavity using KKL model: effects of non-linear thermal radiation and inclined magnetic field, *J. Mol. Liq.* 238 (2017) 485–498, <https://doi.org/10.1016/j.molliq.2017.05.019>.
- [54] A. Wakif, Z. Boulahia, S.R. Mishra, M.M. Rashidi, R. Sehaqui, Influence of a Uniform Transverse Magnetic Field on the Thermo - Hydrodynamic Stability in Water-Based Nanofluids with Metallic Nanoparticles Using the Generalized Buongiorno's Mathematical Model, *Eur. Phys. J. Plus.* 133 (181) (2018) 1–16, <https://doi.org/10.1140/epjp/i2018-12037-7>.
- [55] A. Wakif, Z. Boulahia, A. Amine, I.L. Animasaun, M.I. Afridi, M. Qasim, R. Sehaqui, Magneto-convection of alumina - Water nanofluid within thin horizontal layers using the revised generalized Buongiorno's model, *Front. Heat Mass Transf.* 12 (2019) 1–15, <https://doi.org/10.5098/hmt.12.3>.
- [56] A. Wakif, A. Chamkha, T. Thumma, I.L. Animasaun, R. Sehaqui, Thermal radiation and surface roughness effects on the thermo-magneto-hydrodynamic stability of alumina-copper oxide hybrid nanofluids utilizing the generalized Buongiorno's nanofluid model, *J. Therm. Anal. Calorim.* 143 (2021) 1201–1220, <https://doi.org/10.1007/s10973-020-09488-z>.
- [57] A. Wakif, R. Sehaqui, Generalized differential quadrature scrutinization of an advanced MHD stability problem concerned water-based nanofluids with metal/metal oxide nanomaterials: a proper application of the revised two-phase nanofluid model with convective heating and through, *Numer. Methods Partial. Differ. Equ.* 38 (2022) 608–635, <https://doi.org/10.1002/num.22671>.
- [58] J. Koo, C. Kleinstreuer, Viscous dissipation effects in microtubes and microchannels, *Int. J. Heat Mass Transf.* 47 (2004) 3159–3169, <https://doi.org/10.1016/j.ijheatmasstransfer.2004.02.017>.
- [59] L.N. Trefethen (Ed.), *Spectral Methods in MATLAB*, Society for Industrial and Applied Mathematics, 2000.

- [60] A. Wakif, A novel numerical procedure for simulating steady MHD convective flows of radiative Casson fluids over a horizontal stretching sheet with irregular geometry under the combined influence of temperature-dependent viscosity and thermal conductivity, *Math. Probl. Eng.* 2020 (2020) 1675350, <https://doi.org/10.1155/2020/1675350>.
- [61] A. Wakif, A. Abderrahmane, K. Guedri, B. Bouallegue, P. Kaewmesri, R. Kaewthongrach, S. Channumsin, S. Sreesawet, A. Bumrungrkit, P. Jirawattanapanit, Importance of exponentially falling variability in heat generation on chemically reactive Von Kármán nanofluid flows subjected to a radial magnetic field and controlled locally by zero mass flux and convective heating conditions: a differential quadrature, *Front. Phys.* 10 (988275) (2022) 1–17, <https://doi.org/10.3389/fphy.2022.988275>.
- [62] M. Qasim, M.I. Afridi, A. Wakif, S. Saleem, Influence of variable transport properties on nonlinear radioactive Jeffrey fluid flow over a disk: utilization of generalized differential quadrature method, *Arab. J. Sci. Eng.* 44 (2019) 5987–5996, <https://doi.org/10.1007/s13369-019-03804-y>.
- [63] M. Qasim, Z. Ali, A. Wakif, Z. Boulahia, Numerical simulation of MHD peristaltic flow with variable electrical conductivity and joule dissipation using generalized differential quadrature method, *Commun. Theor. Phys.* 71 (2019) 509–518, <https://doi.org/10.1088/0253-6102/71/5/509>.
- [64] M. Qasim, M.I. Afridi, A. Wakif, T.N. Thoi, A. Hussanan, Second law analysis of unsteady MHD viscous flow over a horizontal stretching sheet heated non-uniformly in the presence of ohmic heating: utilization of gear-generalized differential quadrature method, *Entropy.* 21 (2019) 1–25, <https://doi.org/10.3390/e21030240>.
- [65] A. Wakif, M. Qasim, M.I. Afridi, S. Saleem, M.M. Al-Qarni, Numerical examination of the entropic energy harvesting in a magnetohydrodynamic dissipative flow of Stokes' second problem: utilization of the gear-generalized differential quadrature method, *J. Non-Equilibrium Thermodyn.* (2019) 1–19, <https://doi.org/10.1515/jnet-2018-0099>.
- [66] M.K. Nayak, A. Wakif, I.L. Animasaun, M.S.H. Alaoui, Numerical differential quadrature examination of steady mixed convection nanofluid flows over an isothermal thin needle conveying metallic and metallic oxide nanomaterials: a comparative investigation, *Arab. J. Sci. Eng.* 45 (2020) 5331–5346, <https://doi.org/10.1007/s13369-020-04420-x>.
- [67] T. Thumma, A. Wakif, I.L. Animasaun, Generalized differential quadrature analysis of unsteady three-dimensional MHD radiating dissipative Casson fluid conveying tiny particles, *Heat Transf.* 49 (2020) 2595–2626, <https://doi.org/10.1002/htj.21736>.
- [68] M. Zaydan, N.H. Hamad, A. Wakif, A. Dawar, R. Sehaqui, Generalized differential quadrature analysis of electro-magneto-hydrodynamic dissipative flows over a heated Riga plate in the presence of a space-dependent heat source: The case for strong suction effect, *Heat Transf.* 51 (2022) 2063–2078, <https://doi.org/10.1002/htj.22388>.
- [69] C. Shu, K.H.A. Wee, Numerical simulation of natural convection in a square cavity by SIMPLE-generalized differential quadrature method, *Comput. Fluids.* 31 (2002) 209–226, [https://doi.org/10.1016/S0045-7930\(01\)00024-X](https://doi.org/10.1016/S0045-7930(01)00024-X).
- [70] C. Shu, *Differential quadrature and its application in engineering*, Springer Science & Business Media, London, 2012.
- [71] N. Ishfaq, Z.H. Khan, W.A. Khan, R.J. Culham, Estimation of boundary-layer flow of a nanofluid past a stretching sheet: A revised model, *J. Hydrodyn.* 28 (2016) 596–602, [https://doi.org/10.1016/S1001-6058\(16\)60663-7](https://doi.org/10.1016/S1001-6058(16)60663-7).
- [72] A. Wakif, M. Zaydan, A.S. Alshomrani, T. Muhammad, R. Sehaqui, New insights into the dynamics of alumina-(60% ethylene glycol + 40% water) over an isothermal stretching sheet using a renovated Buongiorno's approach: A numerical GDQLM analysis, *Int. Commun. Heat Mass Transf.* 133 (2022), <https://doi.org/10.1016/j.icheatmasstransfer.2022.105937>.
- [73] N.A. Shah, A. Wakif, E.R. El-Zahar, S. Ahmad, S.-J. Yook, Numerical simulation of a thermally enhanced EMHD flow of a heterogeneous micropolar mixture comprising (60%)-ethylene glycol (EG), (40%)-water (W), and copper oxide nanomaterials (CuO), *Case Stud. Therm. Eng.* 35 (2022), <https://doi.org/10.1016/j.csite.2022.102046>.